Properties of X-Ray Flux of Jets during the 2005 Outburst of Swift J1753.5−0127 Using the TCAF Solution

Arghajit Jana[1], Sandip K. Chakrabarti[1,2], and Dipak Debnath[1]
[1] Indian Center for Space Physics, 43 Chalantika, Garia St. Road, Kolkata, 700084, India; argha@csp.res.in, chakraba@bose.res.in, dipak@csp.res.in
[2] S. N. Bose National Centre for Basic Sciences, Salt Lake, Kolkata, 700106, India

Abstract

Galactic black hole candidate Swift J1753.5−0127 was discovered on 2005 June 30 by the *Swift* Burst Alert Telescope. We study the accretion flow properties during its very first outburst through careful analysis of the evolution of the spectral and the temporal properties using the two-component advective flow (TCAF) paradigm. *RXTE* proportional counter array spectra in 2.5–25 keV are fitted with the current version of the TCAF model fits file to estimate physical flow parameters, such as two-component (Keplerian disk and sub-Keplerian halo) accretion rates, properties of the Compton cloud, probable mass of the source, etc. The source is found to be in harder (hard and hard-intermediate) spectral states during the entire phase of the outburst with very significant jet activity. Since in the TCAF solution the model normalization is constant for any particular source, any requirement of significantly different normalization to have a better fit on certain days would point to an X-ray contribution from components not taken into account in the current TCAF model fits file. By subtracting the contribution using actual normalization, we derive the contribution of X-rays from the jets and outflows. We study its properties, such as its magnitude and spectra. We find that on some days, up to about 32% of X-ray flux is emitted from the base of the jet itself.

Key words: accretion, accretion disks – ISM: jets and outflows – radiation: dynamics – stars: black holes – stars: individual (Swift J1753.5−0127) – X-rays: binaries

1. Introduction

Stellar-mass black holes candidates (BHCs) exhibiting transient behavior generally reside in binaries. They show occasional outbursts of variable duration ranging from a few weeks to months. In between two outbursts, these transient BHCs stay in long periods of quiescence. During the outbursts, compact objects (here, BHCs) accrete matter from their companions via Roche-lobe overflow and/or by wind accretion, which forms a disk-like structure, commonly known as an *accretion disk*. Electromagnetic radiation from radio to γ-rays are emitted from the disk, which makes it observable. It is believed that an outburst is triggered by a sudden rise in viscosity in the disk, which increased the accretion rates in the inner disk causing outbursts (Chakrabarti 2013). Rapid evolution of spectral and temporal properties are observed during an outburst of transient BHCs and these are found to be strongly correlated. In the hardness–intensity diagram (HID; Fender et al. 2004; Debnath et al. 2008) or accretion rate ratio intensity diagram (ARRID; Jana et al. 2016), observed in different states are found to be correlated with different branches. Generally, four spectral states, namely, the hard (HS), hard-intermediate (HIMS), soft-intermediate (SIMS), and soft (SS) states are observed during an outburst. Each state is defined with certain characteristics of spectral and temporal features. HS and HIMS are dominated by non-thermal high energetic radiations with observations of a monotonical rise/fall of low-frequency quasi-periodic oscillations (QPOs), whereas SIMS and SS are dominated by thermal radiations with sporadic QPOs (in SIMS) or no QPOs (in SS; for more details, see Nandi et al. 2012; Debnath et al. 2010, 2013 and references therein). According to Debnath et al. (2017), outbursts are of two types: type-I or classical type, where all spectral states are observed, and type-II or harder type, where SS are absent. The latter type of outbursts are termed as "failed" outbursts. For instance, the 2005 outburst of Swift J1753.5−0127 is of type-II.

The black hole (BH) X-ray spectrum consists of both thermal and non-thermal components. The thermal component is basically a multicolor blackbody that is emitted from the standard Keplerian disk (Shakura & Sunyaev 1973). The non-thermal component is of power-law (PL) type, and it originates from the so-called "hot corona" or "Compton cloud" (Sunyaev & Titarchuk 1980). In the two-component advective flow (TCAF) solution (Chakrabarti & Titarchuk 1995), this corona is identified with the CENtrifugal pressure supported BOundary Layer (CENBOL), which naturally forms behind the centrifugal barrier due to pile-up of the free-falling, weakly viscous (less than critical viscosity), sub-Keplerian (low angular momentum) matter. Soft photons from the Keplerian disk gain energy by repeated inverse-Compton scattering with the hot electron at the CENBOL and emerge as high energetic photons having a power-law distribution in energy. Recently, this TCAF solution has been included in HEASARC's spectral analysis software package XSPEC as an additive table model to fit BH spectra (Debnath et al. 2014, 2015b). Few transient BHCs have been studied by our group during their X-ray outbursts to find a clear picture of the evolution of the physical properties of these sources during their X-ray outbursts (Mondal et al. 2014b, 2016; Debnath et al. 2015a, 2015b, 2017; Chatterjee et al. 2016; Jana et al. 2016; Bhattacharjee et al. 2017; Molla et al. 2017).

Jets and outflows are important features in accretion disk dynamics. According to the TCAF paradigm, the jets and outflows are produced primarily from the CENBOL region (Chakrabarti 1999a; Das & Chakrabarti 1999). If this region remains hot as in hard and hard-intermediate states, jets could be produced, otherwise not. Generally, inflow rates increase as

the object goes from the hard state to the hard-intermediate state; higher outflow rates are also observed in the intermediate states. It is also reported in the literature that blobby jets are possible in intermediate states (Chakrabarti 1999b, 2001; Nandi et al. 2001) due to higher optical depth at the base of the jet, which episodically cools and separates the jets. In softer states, this region is quenched and the outflow rates are reduced (see also Garain et al. 2013). Collimation of the jets could be accomplished by toroidal flux tubes emerging from generally convective disks (Chakrabarti & D'Silva 1994; D'Silva & Chakrabarti 1994). There are several papers in the literature that invoke diverse mechanisms for the acceleration of this topic of discussion, which is beyond the scope of this paper. In this paper, we introduce a new method to estimate X-ray flux, emitted from the base of the jets during the entire period of the 2005 outburst of Swift J1753.5−0127 and compare that with the radio observations.

Radio jets are common in active galactic nucleus (AGN) sources. It has been observed for several Galactic BHCs, such as GRS 1758−258 (Rodríguez et al. 1992), 1E 1740.7−2942 (Mirabel et al. 1992), etc. Compact radio jets have been detected in BHCs, such as GRS 1915+105 (Dhawan et al. 2000) and Cyg X-1 (Stirling et al. 2001). The BHCs GRS 1915+105 (Mirabel & Rodríguez 1994) and GRO J1655−40 (Hjellming & Rupen 1995; Tingay et al. 1995) show superluminal jets. Though jets are prominent in radio, they could be observed in other energy bands, such as X-rays and γ-rays. High-energy γ-ray jets have been observed in Cyg X-1 (Laurent et al. 2011; Jourdain et al. 2012) and V 404 Cyg (Loh et al. 2016). Large-scale, decelerating relativistic X-ray emitting jets have been observed in BHC XTE J1550−564 (Corbel et al. 2002a, 2002b; Kaaret et al. 2006; Tomsick et al. 2003). In this case, radio blobs were predicted to move at relativistic speed, with blobs emitting in X-rays. H 1743−322 also showed a similar X-ray jet (Corbel et al. 2005). Kaaret et al. (2006) reported a large-scale X-ray jet in BHC 4U 1755−33. A relation between IR and X-ray jets has been found in BHC GRS 1915+105 (Eikenberry et al. 1998; Lasso-Cabrera & Eikenberry 2013). The X-ray jet of SS 433 close to the black hole is well known. A correlation between X-ray and radio band intensity in compact jets was first found in BHC GX 339−4 (Hannikainen et al. 1998). The standard correlation is $F_R \propto F_X^b$ with $b \sim 0.6$–0.7 (Corbel et al. 2003; Gallo et al. 2003). This empirical relation is thought to be universal, although for some BHCs, it is observed to have steeper PL with an index of $\sim$1.4 (Jonker et al. 2004; Coriat et al. 2011). Some BHCs also have shown a dual track in the correlation plot. Dual-correlation indices were observed for BHCs GRO J1655−40 (Corbel et al. 2004), H 1743−322 (Coriat et al. 2011), XTE J1752−522 (Ratti et al. 2012), and MAXI J1659−152 (Jonker et al. 2012). Until now, the radio and X-ray correlation study was done using quasi-simultaneous data of radio and X-ray fluxes. Usually, total X-ray flux (disk plus jet) is used for the correlation.

It is reported that jets are emitted in the entire range of electromagnetic spectra: radio to γ-ray. Thus, X-rays emitted from BHCs when jets are present is the net contribution coming from both the jet and the accretion disk. Until now, there was no way to separate the contribution of these two components. In this paper, for the first time, we make an attempt to separate these two components from the total observed X-rays using the unique aspects of spectral studies by the TCAF solution. These aspects are that radiation in the accretion disk component is contributed by the Keplerian disk (dominating the soft X-ray band) and from the "hot Compton cloud" region, i.e., from the CENBOL (dominating the hard X-ray band) and the normalization can be treated as a constant across the spectral states.

Swift J1753.5−0127 was discovered on 2005 June 30 by the *Swift*/BAT instrument at R.A. $= 17^{\rm h}53^{\rm m}28\overset{\rm s}{.}3$, decl. $= -01^\circ27'09\overset{''}{.}3$ (Palmer et al. 2005). BHC Swift J1753.5−0127 has a short orbital period (2.85 hr according to Neustroev et al. 2014; 3.2 ± 0.2 hr according to Zurita et al. 2007). Neustroev et al. (2014) also estimated the mass of the source as $<5\,M_\odot$ and the companion mass to be between 0.17 and $0.25 M_\odot$ with the disk inclination angle $>40^\circ$. On the contrary, Shaw et al. (2016) estimated the mass $>7.4\,M_\odot$. The distance of the source is estimated to be 4–8 kpc (Cadolle Bel et al. 2007). Radio jets are also observed during the 2005 outburst of the source (Fender et al. 2005; Soleri et al. 2010). Several authors have found a radio/X-ray correlation for this source. This does not fall on the traditional correlation track; rather, it shows the power-law index to be steeper, $\sim$1–1.4 (Soleri et al. 2010; Kolehmainen et al. 2016; Rushton et al. 2016).

In Debnath et al. (2017, hereafter Paper I), a detailed study of the spectral and temporal properties of this object during its 2005 outbursts (from 2005 July 2 to October 19) was made. They used the TCAF model fits file to fit the spectra and obtained accretion flow properties of the source during the outburst. Based on the variations of the TCAF model fitted (spectral) physical flow parameters and observed QPO frequencies, the entire 2005 outburst was classified into two harder spectral states, such as HS and HIMS, and these states were observed in the sequence: HS (Ris.) → HIMS (Ris.) → HIMS (decl.) → HS (decl.). They also estimated the mass of the BHC to be in the range of 4.75–5.90 $M_\odot$ or $5.35^{+0.55}_{-0.60}$ $M_\odot$. According to the TCAF solution, model normalization (N) is a function of intrinsic parameters, such as distance, mass, and constant inclination angle of the binary system. So, N is a constant for a particular BHC across, its spectral states unless there is a precession in the disk to change the projected emission surface area or there are some significant outflow or jet activities which so far are not included in the current version (v0.3) of the TCAF model fits file. As reported in Paper I, there are significant deviations of the constant N in a few observations during the outburst. This allows us to estimate the amount of jet flux by separating it from the total X-ray luminosity from our spectral study with the current version of the TCAF solution by keeping model normalization frozen at the lowest observed value. The spectral property of the residual X-ray is also found.

The paper is organized in the following way. In Section 2, we briefly discuss the relation of the jet with spectral states. In Section 3, we also briefly present a method to estimate the jet flux from the total X-ray flux. In Section 4, we present results on our estimated jet flux and its evolution during the entire 2005 outburst of Swift J1753.5−0127. We compare our estimated jet flux with that of the radio fluxes observed during the outburst and study correlation between X-ray and radio jet flux components. Finally, in Section 5, a brief discussion and concluding remarks are presented.

2. Disk–Jet Connection with Spectral States

In general, there are two types of jets: continuous outflows (compact jets) and discrete ejections (blobby jets; Chakrabarti & Nandi 2000; Chakrabarti et al. 2002). In TCAF, CENBOL

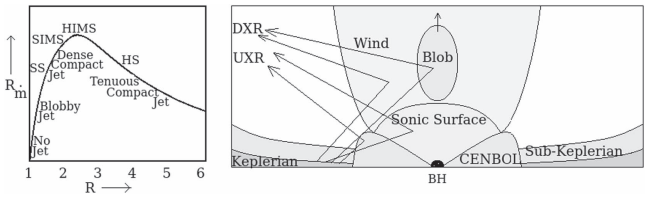

Figure 1. Left panel: variation of ratio $R_{\dot{m}}$ of the outflow and inflow rates as a function of the compression ratio at the shock R. This has a peak at intermediate shock strength. Right panel: examples of Compton scattering of soft photons off the CENBOL, the subsonic part of the outflow and the blobs that may be separated at the intermediate R when the outflow rate is so high that the optical depth will easily allow significant cooling of the outflow base.

acts as a base of the jet (Chakrabarti 1999a). Ejection of the matter depends on the shock location (X_s), compression ratio (R), and inflow rate. A schematic diagram of inflow and outflow is shown in the second panel of Figure 1. Jets move subsonically up to the sonic surface ($\sim 2.5X_s$) and then move away supersonically, thereby reducing its temperature during expansion and emitting in UV and IR to radio (Chakrabarti 1999a, 1999b; Chakrabarti & Manickam 2000, hereafter CM00). The subsonic region will upscatter seed photons from the Keplerian disk and downscatter CENBOL photons contributing to softer X-rays, which we define here as the jet X-ray ($F_{\rm ouf}$) flux in this paper. This does not include the X-rays emitted from interaction of the jet with ambient medium. If the CENBOL is not hot, i.e., the object is not in the hard or hard-intermediate states, compact jets are not possible. However, as the shock moves in due to larger inflow rates and consequent post-shock cooling, as in soft-intermediate states, the outflow rate increases and the subsonic region has a relatively high optical depth (Chakrabarti 1999b). In some outburst sources, Keplerian matter may rise much faster than the sub-Keplerian flow as in the present case (Paper I). Thus, the shock disappears even in HIMS, and blobby jets may arise in HIMS as well.

In presence of high Keplerian accretion rates, CENBOL cools down due to a high supply of the soft photons from the Keplerian disk. Hence, it is quenched and we do not see any jet in this state. The results from this consideration are given in Figure 1 (left panel), where the "generic" variation of the ratio of outflow ($\dot{M}_{\rm out}$) and inflow ($\dot{M}_{\rm in}$) rates ($R_{\dot{m}} = \frac{\dot{M}_{\rm out}}{\dot{M}_{\rm in}}$) with the shock compression ratio (R) is shown. Clearly, the ratio ($R_{\dot{m}}$) is maximum when the Compression ratio is intermediate as in the hard-intermediate and soft-intermediate states. The observed jet in this spectral state is dense compact initially, but becomes increasingly blobby as the transition to the soft-intermediate state is approached. This is due to the rapid cooling of the jet base; the outflowing matter gets separated since even the subsonic flow region suddenly becomes supersonic (Chakrabarti 1999b; Das & Chakrabarti 1999; CM00).

3. Flux and Spectrum of X-Rays from the Base of the Jet

A detailed study of the evolution of the spectral and timing properties for the BHC Swift J1753.5−0127 during its 2005 outburst using the TCAF solution is presented in Paper I. Depending upon the variation of TCAF model fitted physical flow parameters and the nature of QPOs (if present), they classified the entire outburst (from 2005 July 2 to October 19) into two harder (HS and HIMS) spectral states. No signatures of softer states (SIMS and SS) were observed. This could be due to the lack of viscosity that prevented the Keplerian disk from achieving a significant rate close to the black hole. While fitting spectra with the current version (v0.3) of the TCAF solution, the model normalization (N) is found to vary in a very narrow range (1.41–1.81), except for a few days when the radio flux was higher. This may be because of non-inclusion of the jet mechanism in the current TCAF model *fits* file. This motivated us to introduce a new method to detect an X-ray jet and calculate its contribution from the total X-ray flux.

We use 2.5–25 keV *RXTE*/PCA data to calculate the X-ray flux from the base of the outflow. In presence of a jet, the total X-ray flux ($F_{\rm X}$) is contributed from the radiation emitted from both the disk and the base of the jet. So, during the days with significant X-rays in the outflow, we require higher values of the model normalization to fit the spectra, since the present version of our TCAF model fits file is only concerned with the emission from the disk and no contribution from the jets is added. If the jet is absent, a constant or nearly constant TCAF model normalization is capable of fitting the entire outburst (see Chatterjee et al. 2016; Mondal et al. 2016; Molla et al. 2017). In Paper I, TCAF normalization is found to be constant at $\sim$1.6 during the entire 2005 outburst of Swift J1753.5 −0127, except for five observations when it assumed higher values ($\geqslant$2.0) in the initial period of HIMS (decl.). However, in HS (decl.), a minimum normalization of $\sim$1.41 was required to fit spectral data on 2005 September 17 (MJD = 55630.31). We assume that there was very little X-ray jet or outflowing matter on that day, and the entire X-ray flux is contributed only by the accretion disk and CENBOL, i.e., from inflowing matter alone. This is also the theoretical outcome (Chakrabarti 1999b). When we compared the radio data, it was observed that radio flux contributions were also at minimum during these days of observations. To calculate X-ray flux contribution $F_{\rm inf}$ only from the inflow, we refitted all the spectra by freezing model normalization at 1.41. Then, we take the difference of the resulting spectrum from the total flux to calculate jet X-ray flux $F_{\rm ouf}$. In other words, the flux of the jet, relative to MJD = 55630.31, can be written as

$$F_{\rm ouf} = F_{\rm X} - F_{\rm inf}. \quad (1)$$

Here, $F_{\rm X}$ and $F_{\rm inf}$ fluxes (in units of 10^{-9} erg cm^{-2} s^{-1}) are calculated using the "flux 2.5 25.0" command after obtaining the best-fit spectrum in XSPEC. $F_{\rm X}$ is basically the TCAF model flux in the energy range of 2.5–25 keV with free normalization as reported in Paper I, where $F_{\rm inf}$ is the TCAF model flux in the same energy range with a constant normalization, $N = 1.41$.

4. Results

4.1. Evolution of Jet X-Rays

X-ray fluxes from jets or outflow ($F_{\rm ouf}$) are calculated using Equation (1). The variation of the derived jet X-ray flux ($F_{\rm ouf}$) during the entire phase of the 2005 outburst of Swift J1753.5 −0127 is shown in Figure 2(c). To make a comparison, we show the variation of the 4.8 GHz VLA radio flux as reported by Soleri et al. (2010) in Figure 2(d). The first radio observation was $\sim$5 days after the *RXTE*/PCA observation, which missed two initial harder spectral states. Note that the radio flux is at maximum, during the middle of the HIMS, namely, in the late stage of HIMS in the rising phase and early stage of HIMS in the declining phase, precisely as anticipated from the outflow rate

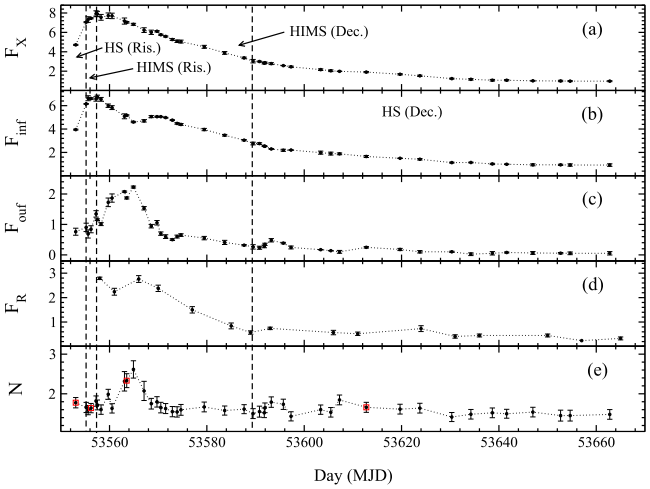

Figure 2. Variations of (a) the total X-ray flux (F_X) and (b) the X-ray flux from the accretion disk (F_{inf}) and (c) from the jet (F_{ouf}) in units of 10^{-9} erg cm^2 s^{-1} are shown. (d) Variation of the radio flux (F_R in mJy) in the 4.8 GHz band of VLA as reported by Soleri et al. (2010) and (e) variation of the TCAF model fitted normalization (N) are shown with day (MJD).

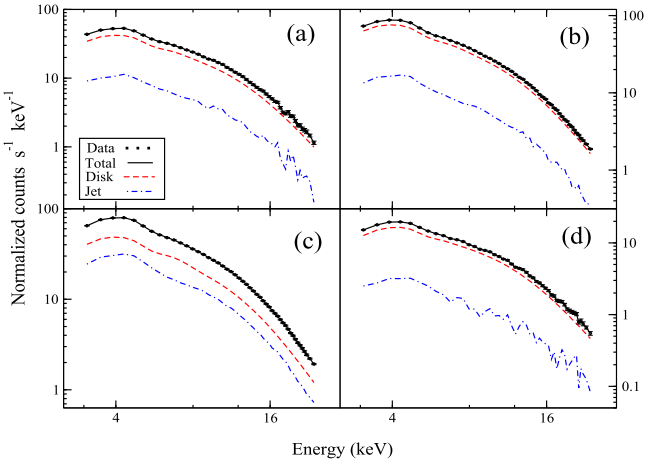

Figure 3. Four spectra selected from four different spectral states, fitted with the TCAF model fits file by keeping model normalization as free (blue curve) or frozen at $N = 1.41$ (red curve). The spectra are from observation IDs: (a) 91094-01-01-00, (b) 91094-01-01-03, (c) 91423-01-02-00, and (d) 91423-01-09-00. Jet X-ray spectra are shown in blue dotted–dashed curves. Note that these spectra are marked as red squares in Figure 2(e).

behavior in Figure 1. Since the object started to return to the hard state, the outflow rate also went down (Figure 2(c)), and thus the radio flux also started to go down (Figure 2(d)). During the initial 5 days (MJD = 53553.05−53557.24), the X-ray flux was completely dominated by the inflowing component (F_{inf}) and reached its peak on 2005 July 7 (MJD = 53557.24), which was the day of the HS to HIMS transition (Paper I). The jet X-ray flux (F_{ouf}) started to increase from the transition day and reached its maxima on 2005 July 13 (MJD = 53564.91). After that, the jet X-ray flux started to decrease; initially, the flux reduced rapidly for the next ∼6 days and then very slowly or roughly became constant until the end of our observation, except a weak local peak, observed on 2005 August 11 (MJD = 53593.23).

The TCAF normalization (N) also shows a behavior similar to the radio flux of the jet as shown by the F_{ouf} plot in Figure 2(c). It was constant in the first few observations. Then it increased and attained maximum value on the same day when F_{ouf} showed peak value on MJD = 53564.91. After that, it decreased rapidly and became almost constant until the end of our observations, starting from ∼MJD = 53570. This additional requirement on N arises from emission of X-rays from the base of the jet, particularly in the subsonic region, which is not included in the present version of the TCAF model fits file.

The four plots in Figures 3(a)–(d) show spectra from four different spectral states (dates marked as red squares in Figure 2 (e)), fitted with free (black solid curve) or frozen (red dashed curve) normalization of the TCAF model. The jet spectrum is also shown (blue dotted–dashed curve). It clearly shows that the jet was becoming stronger as the outburst progressed and was strongest in HIMS (decl.). Then, the contribution from the jet was rapidly reduced as the shock receded farther away in the HS (decl.).

In the strong jet-dominated region (HIMS in the rising and the declining phases), F_{ouf} is observed to be on the order of 10^{-9} erg cm^2 s^{-1}, whereas toward the end of the outburst, when the jet is weak, it decreases by a factor of 100. We also calculated the contribution of the jet in total X-ray emission. On average, the flux of the X-ray jet is ∼12.5% of the total X-rays (F_X). When the jet activity is strong, the contribution rises up to ∼32% (see Table 1). The spectrum of X-ray emission from the jet appears to be harder than the disk spectrum, which is expected when the base of the jet is optically thin. Note also that the spectral slope of the jet component is different with a turnover property at a lower energy than that of the disk, as is expected from an expanded system. Though we did not plot at lower energy, we expect this region to be downscattered radiation emitted from the inflow.

4.2. Correlation between the Radio and X-Ray Jets

The first radio observation of Swift J1753.5−0127 was made with MERLIN on 2005 July 3 at 1.7 GHz (Fender et al. 2005). WRST and VLA also observed the BHC (Soleri et al. 2010). VLA observed the BHC at 1.4 GHz, 4.8 GHz, and 8.4 GHz. The first radio observation was made with VLA on 2005 July 8 (MJD = 53558) with the radio flux $F_R = 2.79$ mJy at 4.8 GHz. After that, F_R slightly decreased on MJD = 53561 before attaining peak on 2005 July 15 (MJD = 53566). X-ray jets attain their peak roughly two days prior to the radio, i.e., on 2005 July 13 (MJD = 53564.91). There is a ∼9 day gap between the second and third radio observations. Therefore, it is hard to find the exact delay between the X-ray jet and the radio peak fluxes, although there is a gap of ∼2 day. Similar to F_{ouf}, F_R also showed a decreasing nature after its peak. F_R decreased rapidly until HIMS (decl.) to the HS (decl.) transition day (MJD = 53589), then decreased slowly, and becomes almost constant from ∼MJD = 53590.

It is known from the literature that there exists a correlation between radio and X-ray wave bands from jets. In Figure 4(a)–(d), we draw an F_R versus F_X plot. We use the results of the available quasi-simultaneous observations of 4.8 GHz VLA and 2.5–25 keV *RXTE*/PCA. In an effort to find a relation, we fit the data with $F_R \sim F_X^b$, where b is a constant. In Figure 4(a), we show the variation between the jet X-ray (F_{ouf}) with radio (F_R) from quasi-simultaneous observations. We obtained $b \sim 0.59 \pm 0.11$. The relation with the X-ray flux from inflow (F_{inf}), shown in Figure 4(b), required an index $b \sim 1.28 \pm 0.11$. The relation of soft X-ray (3 − 9 keV) and radio (Figure 4(c)), which is standard

Table 1
X-Ray Flux from Jets

Obs (1)	ID (2)	MJD (3)	F_X (4)	F_{inf} (5)	F_{out} (6)	% of F_{out} (7)	N (8)
1	X-01-00	53553.05	$4.712^{\pm0.052}$	$3.951^{\pm0.041}$	$0.761^{\pm0.115}$	16.14	$1.775^{\pm0.130}$
2	X-01-01	53555.20	$7.053^{\pm0.049}$	$6.149^{\pm0.035}$	$0.903^{\pm0.137}$	12.81	$1.655^{\pm0.128}$
3	X-01-02	53555.60	$7.323^{\pm0.290}$	$6.636^{\pm0.212}$	$0.687^{\pm0.134}$	9.379	$1.588^{\pm0.117}$
4	X-01-03	53556.19	$7.451^{\pm0.057}$	$6.610^{\pm0.071}$	$0.841^{\pm0.116}$	11.29	$1.639^{\pm0.117}$
5	Y-01-04	53557.24	$7.920^{\pm0.301}$	$6.574^{\pm0.192}$	$1.345^{\pm0.106}$	16.98	$1.816^{\pm0.129}$
6	X-01-04	53557.50	$7.898^{\pm0.271}$	$6.742^{\pm0.156}$	$1.156^{\pm0.027}$	14.63	$1.719^{\pm0.123}$
7	Y-01-00	53558.25	$7.551^{\pm0.299}$	$6.541^{\pm0.162}$	$1.010^{\pm0.048}$	13.37	$1.601^{\pm0.118}$
8	X-02-01	53559.73	$7.721^{\pm0.281}$	$5.995^{\pm0.147}$	$1.725^{\pm0.141}$	22.34	$1.987^{\pm0.126}$
9	X-02-00	53560.51	$7.700^{\pm0.283}$	$5.834^{\pm0.167}$	$1.866^{\pm0.135}$	24.23	$1.632^{\pm0.117}$
10	X-02-02	53561.49	$7.589^{\pm0.271}$	$5.717^{\pm0.152}$	$1.872^{\pm0.119}$	24.67	$2.141^{\pm0.119}$
11	Y-02-00	53563.07	$7.167^{\pm0.315}$	$5.090^{\pm0.209}$	$2.076^{\pm0.021}$	28.96	$2.315^{\pm0.244}$
12	Y-02-05	53563.52	$7.040^{\pm0.078}$	$5.172^{\pm0.051}$	$1.869^{\pm0.033}$	26.54	$2.331^{\pm0.175}$
13	Y-02-06	53564.91	$6.830^{\pm0.102}$	$4.602^{\pm0.054}$	$2.228^{\pm0.033}$	32.62	$2.614^{\pm0.218}$
14	Y-03-00	53567.09	$6.231^{\pm0.242}$	$4.701^{\pm0.102}$	$1.530^{\pm0.056}$	24.56	$2.072^{\pm0.241}$
15	Y-03-02	53568.57	$6.006^{\pm0.223}$	$5.064^{\pm0.088}$	$0.942^{\pm0.058}$	15.68	$1.750^{\pm0.133}$
16	Y-03-03	53569.75	$6.111^{\pm0.071}$	$5.056^{\pm0.050}$	$1.054^{\pm0.074}$	17.25	$1.796^{\pm0.130}$
17	Y-03-04	53570.54	$5.755^{\pm0.061}$	$5.058^{\pm0.028}$	$0.697^{\pm0.056}$	12.11	$1.652^{\pm0.133}$
18	Y-03-05	53571.52	$5.579^{\pm0.057}$	$4.980^{\pm0.024}$	$0.599^{\pm0.061}$	10.74	$1.627^{\pm0.126}$
19	Y-03-06	53572.91	$5.261^{\pm0.091}$	$4.761^{\pm0.035}$	$0.500^{\pm0.026}$	9.510	$1.550^{\pm0.129}$
20	Y-04-00	53573.89	$5.082^{\pm0.122}$	$4.481^{\pm0.064}$	$0.600^{\pm0.047}$	11.82	$1.542^{\pm0.130}$
21	Y-04-01	53574.67	$5.049^{\pm0.152}$	$4.394^{\pm0.078}$	$0.650^{\pm0.044}$	12.88	$1.594^{\pm0.135}$
22	Y-04-06	53579.45	$4.510^{\pm0.154}$	$3.960^{\pm0.098}$	$0.550^{\pm0.056}$	12.20	$1.668^{\pm0.123}$
23	Y-05-01	53583.65	$3.880^{\pm0.140}$	$3.471^{\pm0.071}$	$0.409^{\pm0.069}$	10.54	$1.577^{\pm0.115}$
24	Y-06-00	53587.64	$3.367^{\pm0.079}$	$3.050^{\pm0.058}$	$0.318^{\pm0.021}$	9.436	$1.612^{\pm0.113}$
25	Y-06-01	53589.49	$3.027^{\pm0.179}$	$2.764^{\pm0.118}$	$0.263^{\pm0.073}$	8.696	$1.500^{\pm0.125}$
26	Y-06-05	53590.80	$2.992^{\pm0.045}$	$2.758^{\pm0.071}$	$0.234^{\pm0.051}$	7.816	$1.550^{\pm0.138}$
27	Y-06-06	53591.79	$2.824^{\pm0.084}$	$2.544^{\pm0.037}$	$0.279^{\pm0.045}$	9.907	$1.520^{\pm0.121}$
28	Y-06-07	53591.92	$2.870^{\pm0.069}$	$2.524^{\pm0.025}$	$0.345^{\pm0.037}$	12.05	$1.646^{\pm0.122}$
29	Y-06-03	53593.22	$2.777^{\pm0.097}$	$2.297^{\pm0.041}$	$0.479^{\pm0.055}$	17.27	$1.790^{\pm0.131}$
30	Y-07-00	53595.71	$2.572^{\pm0.014}$	$2.185^{\pm0.087}$	$0.387^{\pm0.023}$	15.03	$1.735^{\pm0.128}$
31	Y-07-01	53597.29	$2.448^{\pm0.075}$	$2.205^{\pm0.024}$	$0.244^{\pm0.048}$	9.951	$1.432^{\pm0.115}$
32	Y-08-01	53603.38	$2.155^{\pm0.087}$	$1.984^{\pm0.132}$	$0.171^{\pm0.006}$	7.919	$1.600^{\pm0.117}$
33	Y-08-02	53605.46	$2.042^{\pm0.088}$	$1.905^{\pm0.125}$	$0.137^{\pm0.007}$	6.713	$1.533^{\pm0.119}$
34	Y-08-03	53607.25	$1.982^{\pm0.022}$	$1.882^{\pm0.077}$	$0.099^{\pm0.048}$	5.009	$1.846^{\pm0.123}$
35	Y-09-00	53612.75	$1.903^{\pm0.064}$	$1.655^{\pm0.087}$	$0.247^{\pm0.025}$	13.01	$1.658^{\pm0.126}$
36	Y-10-00	53619.69	$1.678^{\pm0.069}$	$1.501^{\pm0.021}$	$0.177^{\pm0.036}$	10.57	$1.612^{\pm0.123}$
37	Y-11-00	53623.76	$1.518^{\pm0.071}$	$1.417^{\pm0.065}$	$0.101^{\pm0.041}$	6.649	$1.638^{\pm0.122}$
38	Y-12-00	53630.31	$1.229^{\pm0.049}$	$1.130^{\pm0.042}$	$0.100^{\pm0.019}$	8.188	$1.414^{\pm0.114}$
39	Y-12-01	53634.24	$1.156^{\pm0.079}$	$1.138^{\pm0.031}$	$0.022^{\pm0.045}$	1.901	$1.484^{\pm0.121}$
40	Y-13-00	53638.64	$1.064^{\pm0.081}$	$1.016^{\pm0.056}$	$0.052^{\pm0.056}$	4.876	$1.519^{\pm0.123}$
41	Y-13-01	53641.59	$1.066^{\pm0.063}$	$0.987^{\pm0.027}$	$0.078^{\pm0.017}$	7.361	$1.496^{\pm0.111}$
42	Y-14-00	53646.97	$1.005^{\pm0.042}$	$0.942^{\pm0.083}$	$0.063^{\pm0.047}$	6.258	$1.538^{\pm0.121}$
43	Y-15-00	53652.66	$0.985^{\pm0.071}$	$0.941^{\pm0.052}$	$0.055^{\pm0.023}$	5.640	$1.450^{\pm0.137}$
44	Y-15-01	53654.62	$0.973^{\pm0.054}$	$0.924^{\pm0.099}$	$0.051^{\pm0.045}$	5.301	$1.450^{\pm0.136}$
45	Y-16-01	53662.76	$0.969^{\pm0.052}$	$0.921^{\pm0.108}$	$0.052^{\pm0.056}$	5.332	$1.480^{\pm0.122}$

Note. Average values of 90% confidence ± values obtained using the "err" task in XSPEC are placed as superscripts of fitted parameter values. $X = 91094\text{-}01$ and $Y = 91423\text{-}01$ are the prefixes of observation IDs. Total X-ray flux, accretion disk X-ray flux, and jet X-ray flux in 2.5–25 keV are in the units of 10^{-9} erg cm^{-2} s^{-1}.

practice, yields $b \sim 1.05 \pm 0.14$. When we use F_R and total F_X in the 2.5–25 keV range, we find $b \sim 1.13 \pm 0.12$ (Figure 4(d)).

From these plots we conclude that the entire X-ray (sum of those from inflow and outflow) is well correlated only at lower fluxes, be it in the 3–9 keV range (Figure 4(c)) or in the 2.5–25 keV range (Figure 4(d)). However, if we consider outflow X-ray flux (F_{out}) instead of F_X, then the correlation of F_{out} versus F_R (Figure 4(a)) is found to be weak. However, a good correlation is obtained between F_R and the X-ray flux from the inflow (F_{inf}) at all levels of flux (Figure 4(b)). It is possible that the nature of the jet deviates from compactness as the intermediate state is approached. This behavior is compatible with the observed fact that the compact jets are generally well correlated with the radio flux, while the blobby jets are not.

Swift J1753.5−0127 is less luminous in radio as compared to other BHCs (Soleri et al. 2010). In fact, even during the strong jet observation, the total X-ray flux is not entirely contributed by the jets. A large contribution always comes from the accretion disk. This may be the reason behind not fitting our result with the standard b (0.6–0.7). Rushton et al. (2016) also found a similar result. They found the correlation index to be $\sim 0.99 \pm 0.12$ in soft (0.6–10 keV) and $\sim 0.96 \pm 0.06$ in hard (15–150 keV) X-ray bands using the data of *Swift*/XRT and *Swift*/BAT instruments, respectively.

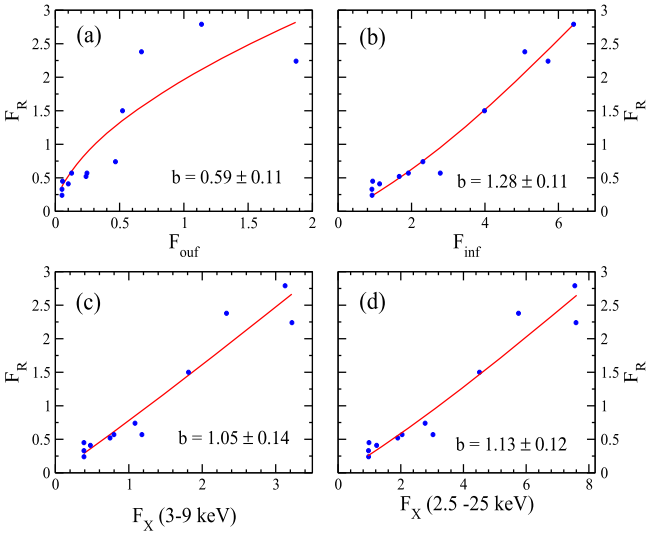

Figure 4. Correlation plots of (a) 2.5–25 keV outflow X-ray ($F_{\rm ouf}$), (b) 2.5–25 keV inflow X-ray ($F_{\rm ouf}$), (c) 3–9 keV total X-ray ($F_{\rm X}$), and (d) 2.5–25 keV total X-ray ($F_{\rm X}$) fluxes with radio (VLA 4.8 GHz) fluxes using quasi-simultaneous observations are shown.

5. Discussions and Concluding Remarks

In this paper, we use a novel approach to obtain the spectral evolution of the X-rays from the outflow component of Swift J1753.5−0127 during its 2005 outburst by exploiting the fact that the normalization of a TCAF fit having X-ray contributions from an inflow remains constant across the states. We use the 2.5–25 keV *RXTE*/PCU2 data of BHC Swift J1753.5−0127 during its 2005 outburst. Much higher normalization values were required to fit spectra on a few days belonging to HIMS (decl.). Assuming the minimum TCAF model normalization, 1.41, obtained on 2005 September 17 (MJD = 55630.31) to be contributed from the 2.5–25 keV range of flux from accretion flows only, we estimated the outflow contribution in the rest of the observations. This was done by separating accretion disk spectrum and flux ($F_{\rm inf}$) from the total spectrum and flux by refitting all spectra, keeping normalization frozen at 1.41. The X-ray flux ($F_{\rm ouf}$) contribution from the outflow was obtained using Equation (1). Time dependence of the X-ray flux and the spectrum from the outflow thus obtained and the flux variation appeared to be similar to the observed radio flux data (see Figure 2(d)).

The variations of $F_{\rm inf}$ and $F_{\rm ouf}$ showed that although initially disk flux increased rapidly and attained its maximum on 2005 July 7 (MJD = 53557.24), the jet flux stays roughly constant. Starting from the time when the $F_{\rm inf}$ was maximum, the jet flux also started to increase and attained its maximum on 2005 July 13 (MJD = 53564.91), when the spectral state changed from hard to hard intermediate. In the declining phase, the jet flux decreased and became roughly constant in the later phase of the outburst and finally became negligible. If we interpret that the radio intensity is directly related to the outflow rate, then it should follow the nature of outflow rate ($\dot{m}R_{\dot{m}}$, where $R_{\dot{m}}$ is the variation, as in Figure 1) that was predicted by Chakrabarti (1999a, 1999b) in the presence of shocks. Here, $\dot{m}$ is the sum of the disk and halo component rates that increased from HS to HIMS (Mondal et al. 2014b, 2016; Debnath et al. 2015a, 2015b; Jana et al. 2016; Molla et al. 2017).

In deriving the properties of the X-rays from the jets, we assumed that the significant variation of the TCAF model normalization (N) is entirely due to the variation in jet contribution in X-ray. Since the outflow rate is supposed to increase in HIMS, it is likely that the X-ray contribution would also go up. We needed $N = 2.61$ (maximum) on MJD = 53564.91 for fitting, when $F_{\rm ouf}$ is observed to be maximum. Correlation between these two is good until the compactness of the jet is maintained. Higher outflow rates may have caused blobbiness (Chakrabarti 1999b, 2000), and the variation of the outflow contribution with radio was no longer well correlated at higher flux. During the radio jet-dominated region, i.e., HIMS (decl.), the X-ray jet had a flux of around of 10^{-9} erg cm^2 s^{-1}, whereas during the declining phase, the flux drops to $\sim 10^{-11}$ erg cm^2 s^{-1}, which is about 100 times lower. There are a few examples of X-ray flux measurements of inner jets. For example, Nandi et al. (2005) showed that the X-ray flux from the jets for BHC SS 433 is around 10^{-10} erg cm^2 s^{-1} in the 3–25 keV energy band. For 4U 1755−33, the X-ray flux from the jet is observed to be around 10^{-16} erg cm^2 s^{-1} in the quiescent state (Angelini & White 2003).

In the later part of the 2005 outburst of the BHC Swift J1753.5−0127, radio flux (F_R) was found to be about constant at its lower value (∼0.4 mJy). Toward of the end of our observations, jets may be moderately stronger in radio but weaker in the X-ray band. Overall, jet X-ray contribution is found to be at ∼12.5% over the total X-ray. When the jet is strong, i.e., in the HIMS, the outflow contribution is about 32% of that of the inflow contribution, surprisingly very similar to the ratio of the flow rates predicted in HIMS (Chakrabarti 1999a). Our result is consistent with what is observed in other similar compact sources.

In the TCAF solution, the jets are considered to emerge out of CENBOL (Chakrabarti 1999a, 1999b), which is the "hot" puffed-up region acting as a Compton cloud. The CENBOL acts as the base of the jet. While CENBOL is the post-shock-compressed matter flowing inward, the matter in the jet is expanding outward and is relatively optically thin. This explains why the spectrum from the jet is flatter. As matter expands and interacts with entangled magnetic fields, it emits radio waves, generally far away from the black hole.

Both the X-ray and the radio emissions from outflow depend on the outflow rate. However, the X-ray component is strong only if the outflow rate is higher, as happens when the object goes to HIMS. Since the shock is weaker, the outflow must be radiation driven, rather than thermal pressure driven. The jets could be blobby when the optical depth is high and the correlation between the two fluxes breaks down. On the other hand, the X-ray emission from the inflow causes $F_{\rm inf}$ to rise also from HS to HIMS. Outflow rate is controlled by the shock strength, i.e., by the compression ratio R (Figure 1). Hence, it is expected that a correlation between $F_{\rm inf}$ and F_R should exist. Since $F_{\rm ouf} \ll F_{\rm inf}$, this translates to a correlation between total $F_{\rm X}$ and F_R. An empirical relation ($F_R \propto F_{\rm X}^b$ with $b \sim 0.6$–0.7) was found by Hannikainen et al. (1998; Corbel et al. 2003; Gallo et al. 2003), although some "outliers" were found to have a steeper power-law index ($b \sim 1.4$; Jonker et al. 2004; Coriat et al. 2011). Using quasi-simultaneous observations of VLA at 4.8 GHz and of the 2.5–25 keV *RXTE*/PCA TCAF model fitted total X-ray flux, we find $b \sim 1.13 \pm 0.12$ for F_R and $F_{\rm X}$, i.e., $F_R \propto F_{\rm X}^{1.13\pm0.12}$. Instead of the 2.5–25 keV total X-ray flux ($F_{\rm X}$), using the 3–9 keV soft X-ray flux, we find a less steep exponent of $b \sim 1.05 \pm 0.14$. Our result is consistent with several other authors, who also have found a steeper exponent

for this particular BHC with $b \sim 1.0$–1.4 (Soleri et al. 2010; Kolehmainen et al. 2016; Rushton et al. 2016). This BHC candidate is less luminous in radio, which may be the reason behind getting a steeper index (Soleri et al. 2010). When $F_{\rm inf}$ and F_R are compared, the index is $\sim 1.28 \pm 0.11$. When $F_{\rm ouf}$ and F_R are compared, $b \sim 0.59 \pm 0.11$. The observed points in the high jet-dominated region are not well correlated in the later case ($F_{\rm ouf}$ versus F_R; see Figure 4(a)). This may be due to the possible blobby nature of the jets in the high flux HIMS (decl.) region of the outburst.

In the future, we would like to estimate X-ray jet fluxes for a few other transient BHCs, such as MAXI J1836−194, XTE J1180+480, etc., where deviations of the constancy of the TCAF model normalization have been observed (see Jana et al. 2016; Chatterjee et al. 2016), using the same method described in this paper as well as persistent sources such as GRS 1915+105, GX 339−4, and V 404 Cyg.

A.J. and D.D. acknowledge the support from the ISRO sponsored RESPOND project fund (ISRO/RES/2/388/2014-15). D.D. also acknowledges support from the DST sponsored Fast-track Young Scientist project fund (SR/FTP/PS-188/2012).

ORCID iDs

Sandip K. Chakrabarti https://orcid.org/0000-0002-0193-1136
Dipak Debnath https://orcid.org/0000-0003-1856-5504

References

Angelini, L., & White, N. E. 2003, ApJL, 586, L71
Bhattacharjee, A., Banerjee, I., Banerjee, A., et al. 2017, MNRAS, 466, 1372
Cadolle Bel, M., Ribó, M., Rodriguez, J., et al. 2007, ApJ, 659, 549
Chakrabarti, S. K. 1999a, A&A, 351, 185
Chakrabarti, S. K. 1999b, InJPB, 73, 931
Chakrabarti, S. K. 2000, CQGra, 17, 2427
Chakrabarti, S. K. 2001, AIPC, 558, 831
Chakrabarti, S. K. 2013, in Proc. Conf. Ser., Vol. 8, Astron. Soc. of India, ed. S. Das (Assam, India), 1
Chakrabarti, S. K., & D'Silva, S. 1994, ApJ, 424, 138
Chakrabarti, S. k., Goldoni, P., Wiita, P. J., et al. 2002, ApJL, 576, L45
Chakrabarti, S. K., & Manickam, S. G. 2000, ApJL, 531, L41
Chakrabarti, S. K., & Nandi, A. 2000, InJPB, 75, 1
Chakrabarti, S. K., & Titarchuk, L. G. 1995, ApJ, 455, 623 (CT95)
Chatterjee, D., Debnath, D., Chakrabarti, S. K, et al. 2016, ApJ, 827, 88
Corbel, S., Fender, R., & Tzioumis, A. 2002a, IAUC, 7795, 2
Corbel, S., Fender, R., & Tzioumis, A. 2002b, Sci, 298, 196
Corbel, S., Fender, R. P., Tomsick, J. A., Tzioumis, A. K., & Tin-gay, S. 2004, ApJ, 617, 1272
Corbel, S., Kaaret, P., Fender, R. P., et al. 2005, ApJ, 632, 504
Corbel, S., Nowak, M. A., Fender, R. P., Tzioumis, A. K., & Markoff, S. 2003, A&A, 400, 1007
Coriat, M., Corbel, S., Prat, L., et al. 2011, MNRAS, 414, 677
Das, T. K., & Chakrabarti, S. K. 1999, CQGra, 16, 3879
Debnath, D., Chakrabarti, S. K., & Mondal, S. 2014, MNRAS, 440, L121
Debnath, D., Chakrabarti, S. K., Nandi, A., et al. 2008, BASI, 36, 151
Debnath, D., Chakrabarti, S. K., & Nandi, A. 2010, A&A, 520, A98
Debnath, D., Chakrabarti, S. K., & Nandi, A. 2013, AdSpR, 52, 2143
Debnath, D., Jana, A., Chakrabarti, S. K., et al. 2017, ApJ, 850, 92
Debnath, D., Molla, A. A., Chakrabarti, S. K., & Mondal, S. 2015a, ApJ, 803, 59
Debnath, D., Mondal, S., & Chakrabarti, S. K. 2015b, MNRAS, 447, 1984
Dhawan, V., Mirabel, I. F., & Rodríguez, L. F. 2000, ApJ, 543, 373
D'Silva, S., & Chakrabarti, S. K. 1994, ApJ, 424, 149
Eikenberry, S. S., Matthews, K., Morgan, H., et al. 1998, ApJL, 494, L61
Fender, R. P., Belloni, T. M., & Gallo, E. 2004, MNRAS, 355, 1105
Fender, R. P., Garrington, S., & Muxlow, T. 2005, ATel, 558, 1
Gallo, E., Fender, R. P., & Pooley, G. G. 2003, MNRAS, 344, 60
Garain, S. K., Ghosh, H., & Chakrabarti, S. K. 2013, ASInC, 8, 11
Hannikainen, D. C., Hunstead, R. W., Campbell-Wilson, D., & Sood, R. K. 1998, A&A, 337, 460
Hjellming, R. M., & Rupen, M. P. 1995, Natur, 375, 464
Jana, A., Debnath, D., Chakrabarti, S. K., et al. 2016, ApJ, 803, 107
Jonker, P. G., Gallo, E., Dhawan, V., et al. 2004, MNRAS, 351, 1359
Jonker, P. G., Miller-Jones, J. C. A., Homan, J., et al. 2012, MNRAS, 423, 3308
Jourdain, E., Roques, J. P., Chauvin, M., & Clark, D. J. 2012, ApJ, 761, 27
Kaaret, P., Corbel, S., Tomsick, J. A., et al. 2006, ApJ, 641, 410
Kolehmainen, M., Fender, R., Jonker, P. G., et al. 2016, AN, 337, 485
Lasso-Cabrera, N. M., & Eikenberry, S. S. 2013, ApJ, 775, 82
Laurent, P., Rodriguez, J., Wilms, J., et al. 2011, Sci, 332, L438
Loh, A., Corbel, S., Dubus, G., et al. 2016, MNRAS, 462, L111
Mirabel, I. F., & Rodríguez, L. F. 1994, Natur, 371, 46
Mirabel, I. F., Rodríguez, L. F., Cordier, B., Paul, J., & Lebrun, F. 1992, Natur, 358, 215
Molla, A. A., Debnath, D., Chakrabarti, S. K., et al. 2016, MNRAS, 460, 3163
Molla, A. A., Debnath, D., Chakrabarti, S. K., et al. 2017, ApJ, 834, 88
Mondal, S., Chakrabarti, S. K., & Debnath, D. 2014a, Ap&SS, 353, 223
Mondal, S., Chakrabarti, S. K., & Debnath, D. 2016, Ap&SS, 361, 309
Mondal, S., Debnath, D., & Chakrabarti, S. K. 2014b, ApJ, 786, 4
Nandi, A., Chakrabarti, S. K., Belloni, T., et al. 2005, MNRAS, 359, 629
Nandi, A., Chakrabarti, S. K., Vadawale, S. V., & Rao, A. R. 2001, A&A, 380, 245
Nandi, A., Debnath, D., Mandal, S., & Chakrabarti, S. K. 2012, A&A, 542, A56
Neustroev, V. V., Veledina, A, Poutanen, J., et al. 2014, MNRAS, 445, 2424
Palmer, D. M., Barthelmey, S. D., Cummings, J. R., et al. 2005, ATel, 546, 1
Ratti, E. M., Jonker, P. G., Miller-Jones, J. C. A., et al. 2012, MNRAS, 423, 2656
Rodríguez, L. F., Mirabel, I. F., & Marti, J. 1992, ApJL, 401, L15
Rushton, A. P., Shaw, A. W., Fender, R. P., et al. 2016, MNRAS, 463, 628
Shakura, N. I., & Sunyaev, R. A. 1973, A&A, 24, 337
Shaw, A. W., Charles, P. A., Casares, J., & Hernández Santisteban, J. V. 2016, MNRAS, 463, 1314
Soleri, P., Fender, R. P., Tudose, V., et al. 2010, MNRAS, 406, 1471
Stirling, A. M., Spencer, R. E., de la Force, C. J., et al. 2001, MNRAS, 327, 1273
Sunyaev, R. A., & Titarchuk, L. G. 1980, ApJ, 86, 121
Tingay, S. J., et al. 1995, Natur, 374, 141
Tomsick, J. A., Corbel, S., Fender, R., et al. 2003, ApJ, 582, 983
Zurita, C., Torres, M. A. P., Durant, M., et al. 2007, ATel, 1130, 1